CrystEngComm

PAPER

View Article Online
View Journal | View Issue

Hydrothermal synthesis of perovskite-type $MTiO_3$ (M = Zn, Co, Ni)/TiO_2 nanotube arrays from an amorphous TiO_2 template†

Cite this: *CrystEngComm*, 2014, **16**, 10280

Xuming Zhang,[a] Biao Gao,[b] Liangsheng Hu,[a] Limin Li,[a] Weihong Jin,[a] Kaifu Huo*[b] and Paul K. Chu*[a]

Received 17th May 2014,
Accepted 31st July 2014

DOI: 10.1039/c4ce00992d

www.rsc.org/crystengcomm

Ordered perovskite-type $MTiO_3$/TiO_2 nanotube arrays (NTAs) (M = Zn, Co, Ni) are prepared by a general hydrothermal route based on amorphous TiO_2 NTAs *via* electrochemical anodization of Ti foil. The as-anodized amorphous TiO_2 is not stable and can react with H_2O in solution producing soluble $Ti(OH)_6^{2-}$ to form anatase nanoparticles (NPs) *via* water-induced dissolution and recrystallization. The pH and salt content in the solution play important roles in the morphology and composition of the hydrothermal products. In the presence of a metal acetate, the reaction between $Ti(OH)_6^{2-}$ and H^+ is dramatically restricted and the reaction proceeds preferentially between $Ti(OH)_6^{2-}$ and M^{2+} (M = Zn, Co, Ni) to produce insoluble $MTiO_3$ NPs which adhere onto the original architecture *in situ* to form perovskite-type $MTiO_3$/TiO_2 NTAs. This study elucidates the role of the amorphous structure in the formation of $MTiO_3$ and provides a general means of synthesizing nanostructured $MTiO_3$.

Introduction

One-dimensional perovskite-type titanates composed of titanium and alkaline earth or transition metals with a common formula of $MTiO_3$ (M = Ba, Sr, Ca, Co, Zn, Ni, *etc.*) have attracted much attention and found many applications in the nanoscale electronics and biomedical industry due to their excellent inherent chemical and physical properties such as photoelectricity, ferroelectricity, piezoelectricity, high dielectric constant, photorefractivity, as well as good biocompatibility.[1–7] Various techniques including sol–gel,[8–10] molten-salt synthesis,[11] and solid-state reactions[12] have been proposed to fabricate nanostructured perovskite-type titanates. In addition, the hydrothermal route[13–16] in the presence of an alkaline mineralizer and a template composed of nanostructured TiO_2 is a facile approach to synthesize nanostructured perovskite-type titanates with the original TiO_2 shape.[13,17,18]

Recently, vertically ordered TiO_2 NTAs prepared by anodization of Ti or Ti alloy foil have attracted increasing attention due to their high photocatalytic activity and excellent biological properties.[5,19–22] The as-anodized TiO_2 NTAs are also good templates for the fabrication of perovskite-type titanate NTAs with excellent physicochemical properties.[23,24] The morphological and structural parameters of the TiO_2 NTAs such as the tube diameter, length, and wall thickness can be controlled by adjusting the anodic voltage, temperature, processing time, and electrolyte composition.[22] $BaTiO_3$, $SrTiO_3$, and $CaTiO_3$ nanostructures have been fabricated by hydrothermal treatment of crystalline TiO_2 NTAs in alkaline hydroxide solutions.[5,14,20] The principle of the hydrothermal reaction involves breaking the Ti–O bonds to form soluble $Ti(HO)_6^{2-}$ species by hydroxy radicals (OH^-) and then combining with metal ions to form the perovskite-type titanate. Unfortunately, since most of the transition metal hydroxides such as $Zn(OH)_2$, $Co(OH)_2$ and $Ni(OH)_2$ are insoluble, the amounts of Zn^{2+}, Co^{2+} and Ni^{2+} are very small while the concentration of OH^- is high. It has been demonstrated that amorphous TiO_2 NTAs have higher chemical reactivity than crystalline TiO_2 NTAs.[25–27] In our previous study,[28] the amorphous TiO_2 NTAs could gradually and spontaneously transform into anatase NPs and finally TiO_2 nanorod arrays (NRAs) composed of compact anatase NPs *via* water-induced dissolution and recrystallization at relative low hydrothermal temperature. Compared with crystalline TiO_2 NTAs, the amorphous TiO_2 NTAs are not stable in water and the unstable TiO_6^{2-} octahedra in amorphous TiO_2 first absorb water molecules *via* the surface hydroxyl groups to form soluble species of $Ti(OH)_6^{2-}$, which can be further dehydrated and precipitated by bridging together and sharing faces to form crystal anatase TiO_2 NPs.[28,29] This self-transformation process provides a novel method to fabricate perovskite-type titanate NTAs in neutral

[a] *Department of Physics and Materials Science, City University of Hong Kong, Tat Chee Avenue, Kowloon, Hong Kong, China. E-mail: paul.chu@cityu.edu.hk*
[b] *Wuhan National Lab for Optoelectronics (WNLO), Huazhong University of Science and Technology, Wuhan 430074, China. E-mail: kfhuo@hust.edu.cn*

† Electronic supplementary information (ESI) available. See DOI: 10.1039/c4ce00992d

solutions by inserting foreign metal ions into the octahedral TiO_6^{2-} group during dehydration.

Herein, we describe a novel means and investigate the mechanism to fabricate aligned transition metal (Zn, Co, Ni, *etc.*) perovskite-type titanate NTAs by hydrothermal treatment of amorphous TiO_2 NTAs with the corresponding metal acetate. The pH and salt content in the solution play important roles in the morphology and composition of the hydrothermal products. This promising route has great potential for producing different kinds of aligned $MTiO_3$ NTAs or other perovskite-type materials in the presence of a self-transforming amorphous template and suitable salts without surfactants under neutral conditions.

Experimental procedure

All chemicals and solvents used in this study were of analytical reagent grade and used as received without purification, and deionized (DI) water was used throughout the experiments.

Firstly, Ti foil (99.6% purchased from Aldrich) was cut into dimensions of 10 × 10 × 1 mm^3, polished with SiC paper, and ultrasonically cleaned in acetone, ethanol, and distilled water sequentially. A conventional two-electrode cell with a direct current (DC) power supply (IT6834, ITECH, China) was employed. Graphite foil and Ti foil served as the cathode and the anode, respectively. The highly ordered amorphous TiO_2 NTAs were fabricated at a constant voltage of 60 V for 1 h in an ethylene glycol solution containing 0.5 wt% ammonium fluoride (NH_4F) and 5 vol% DI water at room temperature. After anodization, the samples were rinsed with distilled water and dried in air. The as-anodized samples were first annealed at 200 °C and then ultrasonically cleaned for 10 min in water to remove residues from the Ti surface formed during anodization. The clean samples were immersed in 40 mL of aqueous solutions (containing different metal acetates) in a 60 mL Teflon-lined autoclave. The autoclave was sealed and heated in an oven to different temperatures for various time durations at a heating rate of 10 °C min^{-1}. After the hydrothermal reaction, the system was cooled to room temperature naturally. The foil was removed from the vessel, ultrasonically washed with DI water for 5 min, and dried in air. The samples were subsequently annealed at different temperatures for 3 h in air at a heating rate of 10 °C min^{-1}.

The samples were characterized using an X-ray diffractometer with Cu K_α radiation (λ = 1.5418 Å) (XRD, Philips X'Pert Pro), a field-emission scanning electron microscope (FE-SEM, FEI Nova 400 Nano) equipped with an energy-dispersive X-ray spectrometer (EDS, Oxford INCA 200 attached to the FE-SEM instrument), a transmission electron microscope (TEM) as well as a high-resolution TEM (JEM-2010 F). The micro-Raman spectra were acquired on a Raman spectrometer (LabRam HR) at room temperature with a 514.5 nm argon laser in the range of 1000–150 cm^{-1} with a resolution of 1 cm^{-1}.

Results and discussion

The ordered TiO_2 NTAs were fabricated by electrochemical anodization of Ti foil in an NH_4F–ethylene glycol solution. Fig. 1a–b depict the top-view and side-view field-emission scanning electron microscopy (FE-SEM) pictures of the as-anodized TiO_2 NTAs prepared at 60 V for 1 h, revealing uniform NTAs with an average inner diameter of 120 nm, a wall thickness of about 15 nm, and a length up to 6.8 μm. The transmission electron microscopy (TEM) image in Fig. 1c further reveals a tubular structure. The diffuse ring of the selected-area electron diffraction (SAED) pattern in the inset of Fig. 1c indicates the amorphous nature of the as-anodized NTAs. The glancing angle XRD pattern (GAXRD, glancing angle of 1°) acquired from the as-anodized NTAs shows no diffraction peaks of any TiO_2 phases, further confirming the amorphous nature of the as-anodized NTAs (Curve 1, Fig. 1d). The as-anodized amorphous NTAs can be crystallized into anatase TiO_2 NTAs (JPDCS no. 21-1271) by thermal treatment in air at 450 °C for 3 h (curve 2, Fig. 1d).

The as-anodized amorphous TiO_2 NTAs on Ti foil are not stable under hydrothermal conditions and gradually self-transform into the anatase phase spontaneously.[28] During the self-transformation, the pH of the solution affects the recrystallization behaviour and morphology of TiO_2. Fig. 2 shows the FE-SEM images of the amorphous TiO_2 NTAs after hydrothermal treatment at 200 °C for 6 h at different pH values. In the HCl solution (pH = 3, Fig. 2a), NRAs composed of compact NPs with a large diameter of 80 nm are observed. In DI water (pH = 6.5, Fig. 2b), NRAs have geometrical dimensions similar to those of NTAs but some small NPs are formed. The corresponding XRD pattern of the NRAs in Fig. 2d shows sharp anatase TiO_2 diffraction peaks. The representative TEM image of a single NR suggests that NPs with a diameter of about 40 nm aggregate to form the NR. The high-resolution TEM image in Fig. 2f reveals single-

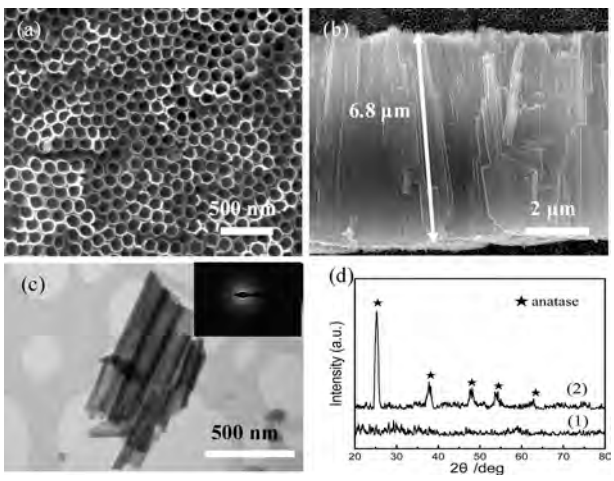

Fig. 1 (a) Top-view and (b) side-view FE-SEM images of TiO_2 NTAs. (c) A typical TEM image of as-anodized TiO_2 NTAs and the corresponding SAED pattern (inset). (d) XRD patterns of as-anodized TiO_2 NTAs before (1) and after (2) calcination in air at 450 °C for 3 h.

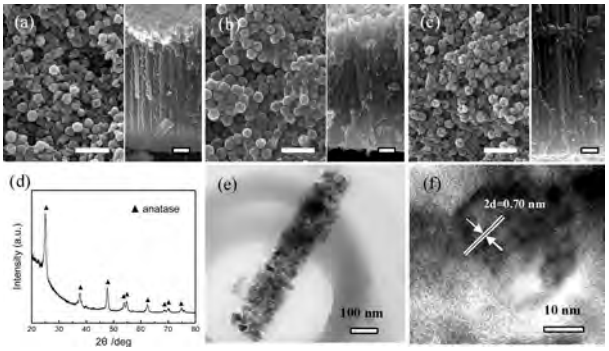

Fig. 2 Top and cross-sectional FE-SEM micrographs of amorphous TiO_2 NTAs after hydrothermal treatment at 200 °C for 6 h in water with different pH values: (a) pH = 3, (b) pH = 6.5, and (c) pH = 11. (d) The corresponding XRD pattern of (b). (e) and (f) TEM and HR-TEM images of an NR and NP in (b). The pH value is adjusted with 1 M HCl and 1 M NaOH and the inset scale bar is 500 nm.

crystalline anatase TiO_2 consistent with the XRD results in Fig. 2d. By further increasing the pH to 11 (Fig. 2c), smaller NPs of 20–30 nm in diameter are observed on the surface and sections of the hydrothermal samples. These NPs are more compact and have a uniform shape compared to the product obtained at low pH. At higher pH (pH = 12.2, 0.02 M NaOH), the NRs are dissolved and nanosheets begin to from (Fig. S1†).

The hydrothermal reaction can be visualized as a water-assisted dissolution and precipitation process between water molecules and amorphous TiO_2 NTAs. Initially, water molecules react with the amorphous TiO_2 to form soluble TiO_6^{2-} octahedra and then precipitation proceeds with the assistance of H^+ forming anatase TiO_2. The overall reaction is described as follows:[28]

$$TiO_x + 4H_2O + (1 - x/2)O_2 \rightarrow Ti(OH)_6^{2-} + 2H^+ \ (1 < x < 2) \quad (1)$$

$$Ti(OH)_6^{2-} + 2H^+ \rightarrow TiO_2\downarrow + H_2O \quad (2)$$

As the hydrothermal reaction proceeds, the amorphous TiO_2 NRAs can be fully converted to anatase TiO_2 NRAs composed of anatase TiO_2 NPs. In this self-transformation process, the concentration of H^+ plays a crucial role in controlling the growth of anatase TiO_2 NPs. Based on chemical eqn (1), the formation of $Ti(OH)_6^{2-}$ can be promoted at high pH due to the combination of H^+ and OH^-. However, reaction (2) forming anatase TiO_2 from $Ti(OH)_6^{2-}$ is prevented at a high pH value. Conversely, at low pH, the growth of anatase TiO_2 NPs is improved as a result of acceleration of reaction (2), thus forming larger TiO_2 NPs as shown in Fig. 2.

In an alkali solution, the perovskite-type titanate NTAs (Ba, Sr and Ca) can also be fabricated in the presence of amorphous TiO_2 NTAs and the corresponding alkaline mineralizer. (Fig. S2†) However, the amorphous TiO_2 NTAs collapse completely after the hydrothermal treatment in a neutral salt solution even at a high concentration, suggesting that reaction (2) is the dominant reaction in the recrystallization process. Thus, in order to precipitate perovskite-type titanate NTAs, reaction (2) should be controlled. A salt containing a transition metal and weak acid radicals, such as acetate, can be used. The weak acid radicals can combine with H^+ to restrict the formation of TiO_2 NPs. On the other hand, the acetate salt provides various metal ion sources to promote the formation of different kinds of perovskite-type titanates. The hydrothermal reactions in the presence of amorphous TiO_2 NTAs and acetate can be described as follows:

$$M(Ac)_2 \leftrightarrow M^{2+} + 2Ac^- \quad (3)$$

$$Ac^- + H^+ \leftrightarrow HAc \quad (4)$$

$$Ti(OH)_6^{2-} + M^{2+} \rightarrow MTiO_3\downarrow + 3H_2O \quad (5)$$

where M is the metal source and Ac is the acid radical of acetate (CH_3COO^-).

To fathom the role of acetate in the formation of perovskite-type titanates on the amorphous TiO_2 NTAs, the growth mechanism is investigated. Here, the acetates of Zn, Co and Ni were used to fabricate the corresponding perovskite-type titanates because of their excellent properties and, more importantly, there have been no reports about the fabrication of $ZnTiO_3$, $CoTiO_3$ and $NiTiO_3$ NTAs by hydrothermal treatment. Fig. 3a–c depict the morphological evolution

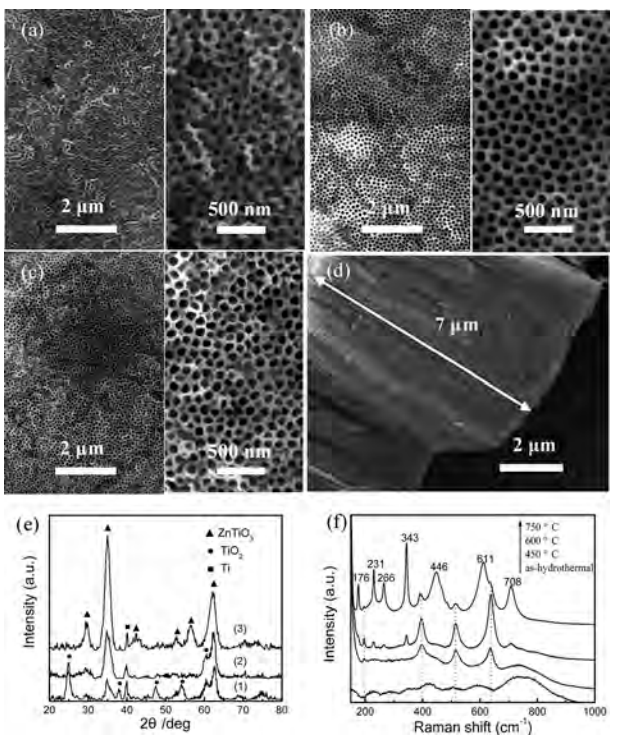

Fig. 3 Low- and high-resolution FE-SEM images of the samples hydrothermally treated with $Zn(Ac)_2$ solutions with different concentrations at 200 °C for 6 h: (a) 0.05 M, (b) 0.2 M and (c) 0.5 M. (d) The corresponding SEM image of (b). (e) XRD patterns of the as-hydrothermal samples after annealing at 450 °C for 3 h in air (1-a, 2-b and 3-c). (f) Raman spectra of the sample in (b).

of the samples hydrothermally treated at 200 °C for 6 h with $Zn(Ac)_2$ solutions at different concentrations. In a 0.05 M $Zn(Ac)_2$ solution (pH = 6.78), the FE-SEM image in Fig. 3a indicates that the double layered NTAs consist of an inner granular tube and an outer continuous skeleton. When the concentration of $Zn(Ac)_2$ is increased to 0.2 M (pH = 6.41), the NPs on the inner wall of the tube aggregate forming a smooth tube with a thickness of about 16 nm. Eventually, nanoporous arrays without boundaries are produced in 0.5 M $Zn(Ac)_2$ (pH = 6.30), as shown in Fig 3b–c. The FE-SEM image of the as-hydrothermal sample (Fig. 3b) indicates that the length of the NTAs is about 7.0 μm without shrinkage compared to the original amorphous TiO_2 NTAs, as shown in Fig. 3d. After annealing at 450 °C for 3 h in air, the XRD patterns of these samples in Fig. 3e exhibit the characteristic diffraction peaks of $ZnTiO_3$ (JCPDS, 39-0190) at 2θ = 30.0°, 35.4°, and 62.4° (ref. 30 and 31) and the relative intensities of the $ZnTiO_3$ peaks increase with $Zn(Ac)_2$ concentrations in the hydrothermal solutions, but those of the anatase TiO_2 phase peaks decrease significantly. The surface Raman spectra in Fig. 3f reveal no significant structural change at 450 °C except for anatase TiO_2 vibration bands at 198, 398, 516 and 638 cm^{-1} (ref. 32) but at 750 °C, Raman shifts at 708, 611, 343, 446, 266, 231 and 176 cm^{-1}, assigned to the vibration modes of $ZnTiO_3$, are observed.[10,32] Despite the high annealing temperature (750 °C), the tubular arrays are preserved (Fig. S3†). However, the crystalline TiO_2 NTAs hydrothermally treated with 0.2 M $Zn(Ac)_2$ and amorphous TiO_2 NTAs hydrothermally treated with 0.2 M $ZnCl_2$ cannot produce $ZnTiO_3$ NTAs as shown in Fig. S3,† suggesting that both the self-dissolved amorphous structure and the weak acid radicals are important to the fabrication of $MTiO_3$ by producing soluble $Ti(OH)_6^{2-}$ and controlling the deposited product.

Fig. 4 shows the morphological and structural evolution of the amorphous TiO_2 NTAs hydrothermally treated with $Co(Ac)_2$ solutions at different concentrations. After the hydrothermal process in 0.05 M $Co(Ac)_2$ (pH = 7.53), a rough tubular surface with many NPs up to 6.5 μm long can be observed in Fig. 4a–b. In the 0.1 M $Co(Ac)_2$ (pH = 7.43) solution, the tubular structure is preserved. The average wall thickness is about 40 nm and the length is 6.6 μm (Fig. 4c–d). When the $Co(Ac)_2$ concentration is increased to 0.2 M (pH = 7.30), porous NTAs with a smooth surface and well-aligned tubular structures from mouth to bottom are still observed (Fig. 4e–f). The XRD patterns of these samples acquired after annealing at 450 °C for 3 h in air show characteristic peaks of $CoTiO_3$ (JCPDS, 77-1373) and the relative intensities of the $CoTiO_3$ peaks are enhanced by increasing the $Co(Ac)_2$ concentration (Fig. 4g). The Raman spectra in Fig. 4h indicate that the surface structure is unstable until at a high annealing temperature of 600 °C. The strong Raman peaks at about 705, 612, 463, 396, 344, 290, 245, and 192 cm^{-1} correspond to vibrations of $CoTiO_3$ and the characteristic peak at 705 cm^{-1} stems from the high-frequency vibration mode (A_{1g}) of octahedral CoO_6 (ref. 33) further confirming that the product is

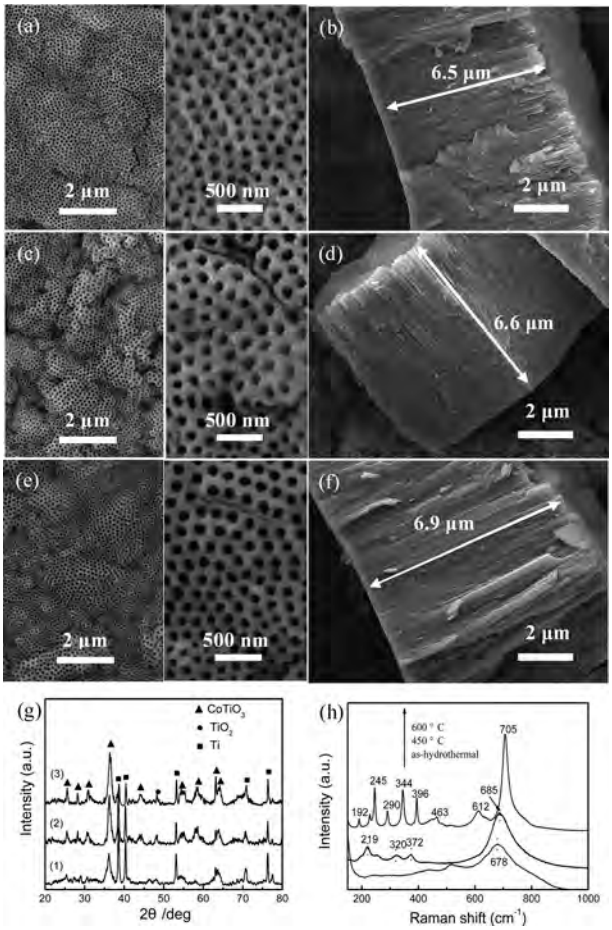

Fig. 4 Top-view and side-view FE-SEM images of the as-hydrothermal samples at 200 °C for 6 h in different concentrations of $Co(Ac)_2$: (a) and (b) 0.05 M; (c) and (d) 0.1 M; (e) and (f) 0.2 M. (g) XRD patterns (1-a, 2-b and 3-c) of the samples after annealing at 450 °C for 3 h in air. (h) Raman spectra of the sample in (e).

$CoTiO_3$ in lieu of a mixture of CoO and anatase TiO_2. The Raman results are in agreement with the XRD patterns. However, when the hydrothermal reaction is carried out in 0.2 M $Co(NO_3)_2$ instead of in $Co(Ac)_2$, a collapsed morphology with a nanorod array shape is again observed (Fig. S4†).

Fig. 5 shows the morphological and structural evolution of as-anodized amorphous TiO_2 NTAs produced by hydrothermal treatment at different temperatures in 0.2 M $Ni(Ac)_2$ (pH = 6.91) for 6 h. A higher or lower concentration of $Ni(Ac)_2$ does not induce the formation of NTAs (Fig. S5†). After hydrothermal treatment at 200 °C for 6 h, the tube diameter shrinks as shown in Fig. 5a. By lowering the hydrothermal temperature to 175 °C, a uniform NT structure (Fig. 5b) with tube lengths up to 6.8 μm can be observed (Fig. 5d). When the temperature is reduced to 150 °C, the NTAs are preserved, as shown in Fig. 5c. The XRD pattern in Fig. 5e suggests that a minimum temperature of 175 °C is needed to form $NiTiO_3$. The diffraction peaks are in good agreement with an orthorhombic lattice for $NiTiO_3$ (JCPDS no. 33-0960).[3] In the range of 150–1000 cm^{-1}, the surface Raman spectra in Fig. 5f reveal an unstable structure unless the annealing temperature is

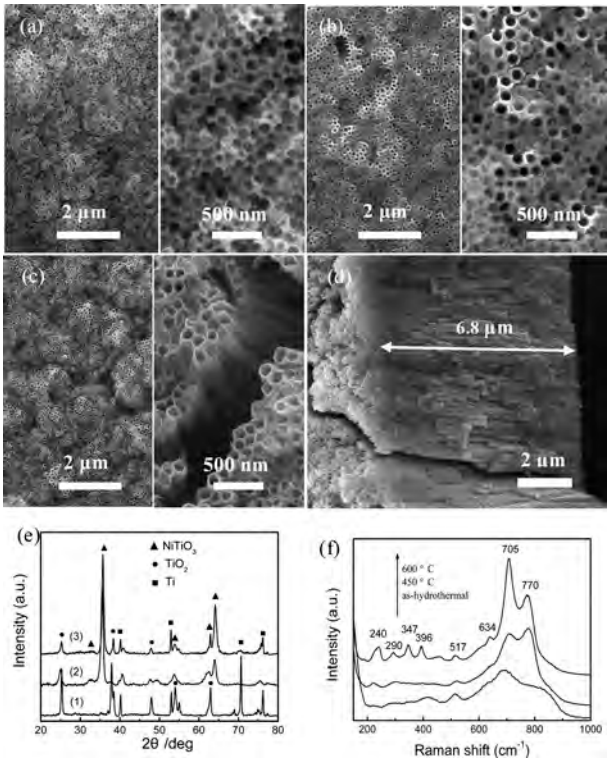

Fig. 5 Low- and high-resolution FE-SEM images of samples hydrothermally treated at different temperatures for 6 h with 0.2 M $Ni(Ac)_2$: (a) 200 °C, (b) 175 °C and (c) 150 °C. (d) The corresponding SEM image of (b). (e) XRD patterns of the samples (1-c, 2-b and 3-a) after annealing at 450 °C for 3 h in air. (f) Raman spectra of (b) at different annealing temperatures.

over 600 °C. The strong broad band at 770 cm^{-1} can be assigned to the stretching vibrations of TiO_6 in $NiTiO_3$ and several bands at around 705, 347, 290, and 240 cm^{-1} correspond to the rhombic structure of $NiTiO_3$.[33–35] Similarly, the NTAs collapse when the acetate is replaced by neutral salts after the hydrothermal treatment (Fig. S5†).

Based on the above experimental results, the mechanism pertaining to the formation of the $MTiO_3$ nanostructures on the amorphous TiO_2 NTAs is illustrated in Scheme 1. Under non-alkaline hydrothermal conditions, the water molecules

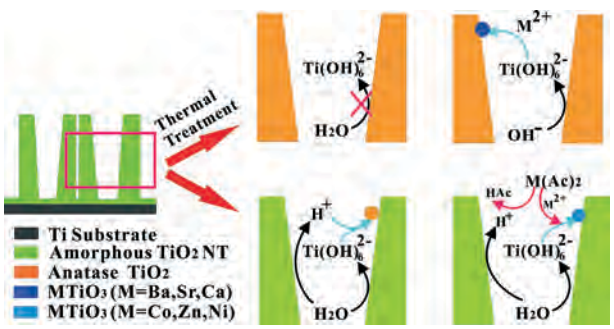

Scheme 1 Schematic illustration of the hydrothermal reactions in the presence of anatase or amorphous TiO_2 NTAs under various hydrothermal conditions.

or salts with weak acid radicals cannot react with the crystalline TiO_2 NTAs due to the stable chemical bonds in anatase TiO_2. Thus, a metal hydroxide solution is needed during the hydrothermal process in order to form $MTiO_3$. However, using the as-anodized amorphous TiO_2 NTAs, water molecules can react with the amorphous TiO_2 to form soluble $Ti(OH)_6^{2-}$. Then, $Ti(OH)_6^{2-}$ reacts with H^+ swiftly leading to the precipitation of anatase TiO_2 NPs. To control the behaviour of H^+ by using the salt containing weak acid radicals, the reaction between $Ti(OH)_6^{2-}$ and H^+ is restricted due to the consumption of H^+ by the weak acid radicals. Therefore, the reaction between $Ti(OH)_6^{2-}$ and M^{2+} is promoted resulting in the production of insoluble $MTiO_3$ NPs on the wall of the tubular structure.

Conclusion

Ordered perovskite-type $MTiO_3/TiO_2$ (M = Co, Zn, Ni) NTAs are fabricated hydrothermally using highly oriented amorphous TiO_2 NTAs as the template and metal acetates as the metal source. During the hydrothermal process, the amorphous TiO_2 NTAs easily self-transform into crystalline TiO_2 by water-assisted dissolution and precipitation and the size of the TiO_2 NPs decreases with increasing pH (<12.2). By introducing the acetate to combine with H^+ preferentially depending on the weak acid radicals, perovskite-type $MTiO_3$ NPs are precipitated on the original tubular wall and form $MTiO_3/TiO_2$ NTAs. The result provides a new method to fabricate perovskite-type $MTiO_3$ without an alkaline mineralizer and insight into the role of the amorphous structure in the fabrication of perovskite-type materials in the hydrothermal process.

Acknowledgements

This work was financially supported by the Guangdong - Hong Kong Technology Cooperation Funding Scheme (TCFS) GHP/015/12SZ and the City University of Hong Kong Applied Research Grant (ARG) no. 9667085.

Notes and references

1 W. Dong, B. Li, Y. Li, X. Wang, L. An, C. Li, B. Chen, G. Wang and Z. Shi, *J. Phys. Chem. C*, 2011, **115**, 3918–3925.
2 Y. Li, X. P. Gao, G. R. Li, G. L. Pan, T. Y. Yan and H. Y. Zhu, *J. Phys. Chem. C*, 2009, **113**, 4386–4394.
3 Y. K. Sharma, M. Kharkwal, S. Uma and R. Nagarajan, *Polyhedron*, 2009, **28**, 579–585.
4 D. A. Wang, Z. G. Guo, Y. M. Chen, J. C. Hao and W. M. Liu, *Inorg. Chem.*, 2007, **46**, 7707–7709.
5 Y. C. Xin, J. Jiang, K. F. Huo, T. Hu and P. K. Chu, *ACS Nano*, 2009, **3**, 3228–3234.
6 K. F. Huo, X. M. Zhang, H. R. Wang, L. Z. Zhao, X. Y. Liu and P. K. Chu, *Biomaterials*, 2013, **34**, 3467–3478.
7 L. Z. Zhao, H. R. Wang, K. F. Huo, X. M. Zhang, W. Wang, Y. M. Zhang, Z. F. Wu and P. K. Chu, *Biomaterials*, 2013, **34**, 19–29.

8 B. A. Hernandez, K. S. Chang, E. R. Fisher and P. K. Dorhout, *Chem. Mater.*, 2002, **14**, 480–482.
9 H. Y. Xu, S. Q. Wei, H. Wang, M. K. Zhu, R. Yu and H. Yan, *J. Cryst. Growth*, 2006, **292**, 159–164.
10 L. Hou, Y. D. Hou, M. K. Zhu, J. L. Tang, J. B. Liu, H. Wang and H. Yan, *Mater. Lett.*, 2005, **59**, 197–200.
11 H. Deng, Y. C. Qiu and S. H. Yang, *J. Mater. Chem.*, 2009, **19**, 976–982.
12 M. T. Buscaglia, C. Harnagea, M. Dapiaggi, V. Buscaglia, A. Pignolet and P. Nanni, *Chem. Mater.*, 2009, **21**, 5058–5065.
13 Y. B. Mao, S. Banerjee and S. S. Wong, *Chem. Commun.*, 2003, 408–409.
14 F. Maxim, P. Ferreira, P. M. Vilarinho and I. Reaney, *Cryst. Growth Des.*, 2008, **8**, 3309–3315.
15 X. Z. Wei, *J. Cryst. Growth*, 2006, **286**, 371–375.
16 U. A. Joshi, S. Yoon, S. Baik and J. S. Lee, *J. Phys. Chem. B*, 2006, **110**, 12249–12256.
17 N. Z. Bao, L. M. Shen, G. Srinivasan, K. Yanagisawa and A. Gupta, *J. Phys. Chem. C*, 2008, **112**, 8634–8642.
18 J. Xie, T. H. Ji, X. H. Yang, Z. Y. Xiao and H. J. Shi, *Solid State Commun.*, 2008, **147**, 226–229.
19 D. Kuang, J. Brillet, P. Chen, M. Takata, S. Uchida, H. Miura, K. Sumioka, S. M. Zakeeruddin and M. Grätzel, *ACS Nano*, 2008, **2**, 1113–1116.
20 D. V. Bavykin and F. C. Walsh, *Titanate and Titania Nanotubes Synthesis, Properties and Applications*, RSC Publishing, 2010.
21 X. M. Zhang, K. F. Huo, L. S. Hu, Z. W. Wu and P. K. Chu, *J. Am. Ceram. Soc.*, 2010, **93**, 2771–2778.
22 X. M. Zhang, K. F. Huo, H. R. Wang, W. R. Zhang and P. K. Chu, *J. Nanosci. Nanotechnol.*, 2011, **11**, 11200–11205.
23 C. A. Grimes and G. K. Mor, *TiO_2 Nanotube Arrays; Synthesis, Properties, and Applications*, Springer, New York, 2009.
24 B. Im, H. Jun, K. H. Lee and J. S. Lee, *CrystEngComm*, 2011, **13**, 7212–7215.
25 D. W. Wang, H. T. Fang, F. Li, Z. G. Chen, Q. S. Zhong, G. Q. Lu and H. M. Cheng, *Adv. Funct. Mater.*, 2008, **18**, 3787–3793.
26 H. Y. Zhu, Y. Lan, X. P. Gao, S. P. Ringer, Z. F. Zheng, D. Y. Song and J. C. Zhao, *J. Am. Chem. Soc.*, 2005, **127**, 6730–6736.
27 E. Lester, P. Blood, J. Denyer, D. Giddings, B. Azzopardi and M. Poliakoff, *J. Supercrit. Fluids*, 2006, **37**, 209–214.
28 K. F. Huo, H. R. Wang, X. M. Zhang, Y. Cao and P. K. Chu, *ChemPlusChem*, 2012, **77**, 323–329.
29 D. A. Wang, L. F. Liu, F. X. Zhang, K. Tao, E. Pippel and K. Domen, *Nano Lett.*, 2011, **11**, 3649–3655.
30 J. Z. Kong, A. D. Li, H. F. Zhai, H. Li, Q. Y. Yan, J. Ma and D. Wu, *J. Hazard. Mater.*, 2009, **171**, 918–923.
31 L. Q. Wang, H. M. Kang, D. F. Xue and C. H. Liu, *J. Cryst. Growth*, 2009, **311**, 611–614.
32 J. Wang and Z. Q. Lin, *Chem. Mater.*, 2008, **20**, 1257–1261.
33 G. Busca, G. Ramis, J. M. G. Amores, V. S. Escribano and P. Piaggio, *J. Chem. Soc., Faraday Trans.*, 1994, **90**, 3181–3190.
34 K. P. Lopes, L. S. Cavalcante, A. Z. Simões, J. A. Varela, E. Longo and E. R. Leite, *J. Alloys Compd.*, 2009, **468**, 327–332.
35 S. H. Chuang, M. L. Hsieh, S. C. Wu, H. C. Lin, T. S. Chao and T. H. Hou, *J. Am. Ceram. Soc.*, 2011, **94**, 250–254.